Polarized reflectivity of β-$Sr_{0.17}V_2O_5$

V. Ta Phuoc,[1] C. Sellier,[2] E. Janod,[2] and C. Marin[3]

[1]*Laboratoire d'Électrodynamique des Matériaux Avancés, CNRS UMR 6157–CEA, Université F. Rabelais, UFR Sciences, Parc de Grandmont, 37200 Tours, France*

[2]*Institut des Matériaux Jean Rouxel (IMN), Université de Nantes, CNRS, 2 rue de la Houssinière, BP32229, 44322 Nantes cedex 3, France*

[3]*DRFMC/SPSMS/IMAPEC–CEA Grenoble, 17 Avenue des Martyrs, 38054 Grenoble Cedex, France*

(Received 4 September 2007; revised manuscript received 15 November 2007; published 21 February 2008)

In order to investigate phonon dynamics, infrared polarized reflectivity was measured along the *b* axis and on the low symmetry *ac* face of a monoclinic β-$Sr_{0.17}V_2O_5$ single crystal. Whereas 11 A_u modes are expected along the *b* axis, only four broad and asymmetric modes are observed. Such a discrepancy with factor group analysis presumably results from the coupling of the phonons with an electronic background. Thus, both reflectivity and optical conductivity, obtained from Kramers-Kronig analysis, were fitted with Fano line shapes. In the *ac* face, almost all the 22 B_u modes predicted by the factor group analysis are observed. Reflectivity spectra are analyzed by using a tensor dispersion formula. To extract phonon parameters, including dipole moments, not predicted by group theory, the model requires us to measure the reflectivity for at least three polarizations. The assignement of high frequency phonon modes is made by comparing bond length and mode frequencies with α-$'NaV_2O_5$ and V_2O_5 and by using the dipole moment directions. Phonon modes assigned to V-O-V rungs stretching show unusually large dampings. We interpret these anomalous dampings as due to charge delocalization within V-O-V rungs. The mean Born effective charge tensors obtained from the model show a clear anisotropy in the *ac* plane.

DOI: 10.1103/PhysRevB.77.075123 PACS number(s): 78.30.Hv, 71.27.+a, 63.20.−e

I. INTRODUCTION

Low dimensional materials show various instabilities, such as spin density wave or charge density waves.[1] Moreover, electronic correlations and transverse interactions are of fundamental importance in such systems since they could lead to insulating ground states or dimensional crossover.[2,3] On the other hand, 3*d* transition metal oxides show a large variety of physical properties because of the interplay between charge, orbital, spin, and lattice degrees of freedom.[4]

$\beta(\beta')$-$A_xV_2O_5$ compounds (A=Na, Ag, Cu, Li, Ca, and Sr) are examples of quasi-one-dimensional transition metal oxides showing puzzling electronic and magnetic properties. These compounds have attracted much attention since a metal-insulator transition (MIT) was observed in β-$A_{x\approx0.33}V_2O_5$ (Refs. 5 and 6), and superconductivity was found in β-$Na_{x\approx0.33}V_2O_5$ and β'-$Cu_{x\approx0.66}V_2O_5$ (Refs. 7 and 8) under pressure. Moreover, a charge order (CO) insulating ground state takes place below the MIT,[9–12] with a transition between different CO patterns under pressure in β-$Sr_{0.33}V_2O_5$.[13] From optical conductivity[10,14,15] and photoemission measurement,[16] it was claimed that charge carriers are small polarons, whereas nonlinear transport properties are very similar to charge density wave systems.[17] The MIT, the charge order pattern, as well as the various magnetic properties are not well understood yet.[6,18–20]

β-$A_xV_2O_5$ belongs to the $C2/m$ space group at room temperature. The *A* cations are randomly distributed over the two sites available in the tunnels formed by the V_2O_5 framework. For $x \geqslant 0.3$, a zigzag order of the *A* cations appears, resulting in a doubling of the unit cell.[12,21] In the $C2/m$ structure, vanadium atoms occupy three different sites, V1, V2, and V3 (Fig. 1). $V1O_6$ and $V3O_5$ polyhedra are arranged in zigzag chains, whereas $V2O_6$ octahedra form a ladder along the *b* axis. Recent extended Hückel tight binding calculations[22] have shown that the adequate *electronic* structure consists in two different nearly orthogonal two-leg ladders running along the *b* axis, namely, V1-O-V3 and V2-O-V2 ladders, as illustrated in Fig. 1.

Since β-$A_xV_2O_5$ are mixed-valence compounds, the valence of the three vanadium sites could be different even at room temperature. Above the MIT temperature, ^{51}V NMR measurements suggest that the charges are spread over V1, V2, and V3 sites for the divalent compounds β-$Ca^{2+}_{0.33}V_2O_5$ and β-$Sr^{2+}_{0.33}V_2O_5$,[6,9] which seems to disagree with Raman experiments[11] on CaV_6O_{15}, suggesting that *d* electrons occupy only the V1 and V3 sites, the V2 one being empty. On the other hand, ^{51}V NMR, ESR measurements, and theoretical results indicate that electrons mainly occupy V1 sites in monovalent β-$Na_{0.33}V_2O_5$.[9,20,23–26]

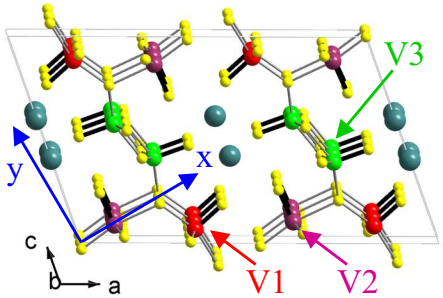

FIG. 1. (Color online) Crystallographic structure in the *ac* plane. The *x* and *y* arrows define the system of axis chosen to measure the polarized reflectivity (R_{00}, R_{45}, R_{90}, and R_{-45}). The black segments correspond to the V-O vanadyl bonds.

The 1 eV peaks observed in the optical conductivity have been assigned to transitions within molecular orbitals formed on V1-O-V3 and V2-O-V2 rungs.[27] Note that this implies that electrons are not located on vanadium sites but are delocalized over the rungs, similarly to NaV_2O_5.[28–30] By following the changes of these peaks as a function of x in β-$Sr_xV_2O_5$ and β-$Na_{0.33}V_2O_5$, it has been proposed that electrons mainly occupy V1-O-V3 rungs for β-$Sr_{0.17}V_2O_5$ and β-$Na_{0.33}V_2O_5$, while V2-O-V2 rungs are progressively filled as x increases. The occupancy of the different vanadium sites or V-O-V rungs is of crucial importance to understand MIT and charge order pattern.

In this paper, we focus on phonon dynamics in a β-$Sr_{0.17}V_2O_5$ single crystal. This compound is isoelectronic and isostructural to β-$Na_{0.33}V_2O_5$, but does not show a MIT transition. Along the b axis, experimental data have been fitted with Fano profiles in order to take into account phonon line shape asymmetry presumably due to coupling with an electronic continuum. In the ac face, we used tensor dispersion formula to accurately extract phonon parameters, including dipole moments and mean Born effective charge tensors. Phonon modes are assigned by comparison with experiments and lattice dynamics calculation on NaV_2O_5 and V_2O_5. Possible phonon anomalies, such as unusual phonon dampings are discussed as a signature of charge delocalization over the rungs. In Sec. II, sample preparation and temperature dependent optical reflectivity experiment are described. The tensor dispersion model is recalled in Sec. III. Results are discussed in Sec. IV.

II. EXPERIMENTAL DETAILS

Polycrystalline β-$Sr_{0.17}V_2O_5$ was synthesized as described in Ref. 5. The powder was compacted isostatically under 1200 bar so as to obtain a 50 mm long feed rod. The β-$Sr_xV_2O_5$ crystals have been grown by a traveling solvent floating zone technique using a commercial Crystal System Inc. image furnace FZ-T-10000-H-VI-P-G. The melting zone was stabilized in between four low power halogen lamps of 150 W (one-third of the nominal power was sufficient to melt the compound) under an oxygen partial pressure of 40–100 ppm in argon flow. The growth rate was set to 2 mm/h, and the crystallized rod obtained was 45 mm long. The SVO phase was checked by x-ray powder diffraction, and the bulk crystal quality tested by neutron diffraction, using a D23 spectrometer (ILL reactor/Grenoble). We obtained large single grains, more than 15 mm along the b axis with a platelet shape (bc planes) of typically 0.5 mm of thickness. The b axis was found as the growth direction. Several grains were observed in the crystallized rod section with a common b axis and a small misorientation of 4° along the c axis between neighboring grains. The Sr: V ratio measured by energy dispersive x-ray analysis ($0.17 \pm 0.01:2$) is close to the expected value (1/6:2). The single crystal stoichiometry is further confirmed by cell parameter determination (a=15.51 Å, b=3.62 Å, c=10.08 Å, and β=109.37°), which agrees with values determined on polycrystalline samples.[31] As grown β-$Sr_{0.17}V_2O_5$ single crystals were cut with a wire saw and used for the following physical studies.

Near normal incidence reflectivity spectra were measured with a Bruker IFS 66v/S in the range of 50–22 000 cm^{-1}. The sample was polished up to an optical grade (0.25 μm). For the ac face of the crystal, polarized reflectivity spectra were measured with the electric field parallel and perpendicular to the V2-O-V2 rungs, and at 45° and −45° of this direction. After the initial measurement, the samples were coated *in situ* with a gold film and remeasured for all polarizations. These additional data were used as reference mirrors to calculate the reflectivity in order to take into account light scattering on the surface of the sample.

III. DISPERSION ANALYSIS

A. Dielectric tensor

For a monoclinic crystal structure $[\mathbf{b} \perp (\mathbf{a},\mathbf{c}), (\hat{\mathbf{a}},\mathbf{c}) \neq 90°]$, the only crystallographic axis that coincides with a principal dielectric axis is the b axis. Indeed, for the low symmetry (ac) face, the principal dielectric axes cannot be determined by symmetry arguments. Usually, they do not correspond to crystallographic axes, and depend on frequency.[32] Thus, since usual scalar dispersion analysis can be used to investigate dielectric properties for the electric field polarized along the b axis, tensor dispersion formulas are require to analyze optical properties for the electric field lying in the (ac) plane.

Along the b axis, the complex dielectric function can be obtained by a Kramers-Kronig analysis or by a usual Drude-Lorentz fit,

$$R_b(\omega) = \left| \frac{1 - \sqrt{\epsilon_b(\omega)}}{1 + \sqrt{\epsilon_b(\omega)}} \right|^2, \tag{1}$$

with

$$\epsilon_b(\omega) = \epsilon_b^{\infty} + \sum_i \frac{\omega_{p,i}^2}{\omega_{\mathrm{TO},i}^2 - \omega^2 - i\gamma_i\omega}, \tag{2}$$

where the summation is over the A_u modes, $\omega_{p,i}$, $\omega_{\mathrm{TO},i}$, and γ_i are the effective plasma frequency, the frequency, and the damping of the ith A_u mode, respectively. Note that a Drude term can possibly be added to take free charge carriers into account.

In the (ac) plane, choosing an orthogonal system of coordinates (xOz), the 2D dielectric tensor reads

$$\hat{\epsilon}_{ac} = \begin{pmatrix} \epsilon_{xx} & \epsilon_{xz} \\ \epsilon_{xz} & \epsilon_{zz} \end{pmatrix}. \tag{3}$$

The dispersion formula is[32,33]

$$\hat{\epsilon}_{ac}(\omega) = \hat{\epsilon}_{ac}^{\infty} + \sum_i \frac{\omega_{p,i}^2}{\omega_{\mathrm{TO},i}^2 - \omega^2 - i\gamma_i\omega} \times \begin{pmatrix} \cos^2\theta_i & \cos\theta_i \sin\theta_i \\ \cos\theta_i \sin\theta_i & \sin^2\theta_i \end{pmatrix}, \tag{4}$$

where the summation is over the B_u modes, $\omega_{p,i}$, $\omega_{\mathrm{TO},i}$, and γ_i are the effective plasma frequency, the frequency, and the damping of the ith B_u mode, respectively. The additional

parameter θ_i is the angle between the dipole moment of the ith B_u mode and the x axis. Thus, the optical conductivity tensor is

$$\hat{\sigma}_{ac}(\omega) = \frac{\omega}{4\pi} \mathrm{Im}[\hat{\epsilon}_{ac}(\omega)]. \quad (5)$$

The complex reflectivity tensor reads

$$\hat{r}_{ac}(\omega) = [I - \sqrt{\hat{\epsilon}_{ac}(\omega)}] \cdot [I + \sqrt{\hat{\epsilon}_{ac}(\omega)}]^{-1}, \quad (6)$$

where I is the unity matrix and the exponent -1 means the inverse matrix. Thus, for a direction $\mathbf{e}$ of the electric field in the (ac) plane, the reflectivity reads

$$R_{ac}(\omega, \mathbf{e}) = |\hat{r}_{ac}(\omega)\mathbf{e}|^2. \quad (7)$$

As pointed out by Kuz'menko *et al.*,[34] reflectivity spectra for at least three polarizations are required to obtain unambiguously the dielectric tensor in the ac plane. The authors successfully extracted phonon parameters ($\omega_{p,i}$, $\omega_{\mathrm{TO},i}$, γ_i, and θ_i) of CuO (Ref. 33) and α-Bi_2O_3 (Ref. 34) with the measurement of the reflectivities $R_{00}(\omega)$, $R_{45}(\omega)$, and $R_{90}(\omega)$, namely, for the electric field oriented at 0°, 45°, and 90° of the x axis, respectively. Using Eqs. (4) and (7), one can write

$$R_{00}(\omega) = |r_{xx}(\omega)|^2 + |r_{xz}(\omega)|^2, \quad (8)$$

$$R_{45}(\omega) = (|r_{xx}(\omega) + r_{xz}(\omega)|^2 + |r_{xz}(\omega) + r_{zz}(\omega)|^2)/2, \quad (9)$$

$$R_{90}(\omega) = |r_{xz}(\omega)|^2 + |r_{zz}(\omega)|^2. \quad (10)$$

The model also implies

$$R_{00}(\omega) + R_{90}(\omega) = R_{-45}(\omega) + R_{45}(\omega), \quad (11)$$

where $R_{-45}(\omega)$ is the reflectivity for an angle of $-45°$ between the electric field and the x axis. Note that the validity and the accuracy of the model can be checked by comparing the reflectivity calculated with the dielectric tensor and $R_\theta(\omega)$ measured for any angle.

B. Effective charge tensor

In the ac plane, the Born effective charge tensor $\hat{Z}_k^*$ of an atom k and the phonon parameters are related by

$$\sum_k \frac{\hat{Z}_k^{*2}}{m_k} = \frac{v_c}{4\pi} \sum_i \omega_{p,i}^2 \begin{pmatrix} \cos^2\theta_i & \cos\theta_i \sin\theta_i \\ \cos\theta_i \sin\theta_i & \sin^2\theta_i \end{pmatrix}, \quad (12)$$

where m_k is the mass of the kth atom and v_c is the unit cell volume. The left term is a summation over all the atoms of the unit cell, and the right term corresponds to a summation over all the B_u modes. For binary compounds, the combination of Eq. (11) and the acoustic sum rule $\Sigma_k \hat{Z}_k^* = 0$ allows us to determine the average Born effective charge tensor for each atomic species. For ternary compounds, the number of unknown parameters exceeds the number of equations. Therefore, Z_k^* cannot usually be determined. However, if the amount of a certain atomic specie is small enough in the unit cell, or if a certain atomic species is heavier enough compared to the other, it can be neglected. In this case, an approximate average effective charge tensor can be determined for the two other species.

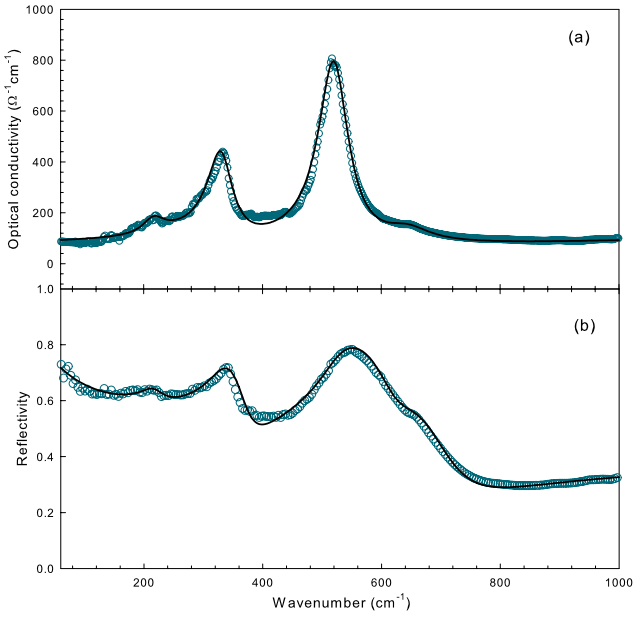

FIG. 2. (Color online) Optical conductivity obtained from the Kramers-Kronig analysis (a) and reflectivity (b) along the b axis. Open circles are experimental curves. Solid lines are the fits with Fano line shapes (see text).

IV. RESULTS

A. b-axis phonon dynamics

The b-axis reflectivity and the optical conductivity deduced by the Kramers-Kronig analysis are shown in Fig. 2. Below the phonon modes, an electronic background is observed. Note that a broad midinfrared peak is found at 4000 cm^{-1} (not shown in the figure). The factor group analysis (FGA) leads to

$$\Gamma = 11A_u + 22B_u + 22A_g + 11B_g. \quad (13)$$

The IR active modes are 11 A_u along the b axis and $22B_u$ in the (a,c) plane. The 22 A_g and 11 B_g are Raman active. Of the 11 predicted A_u modes, only two large modes at 333 and 522 cm^{-1} and two very broad peaks at 220 and 647 cm^{-1} are found. Such a discrepancy with FGA as well as asymmetric line shapes of some phonon modes suggest an interaction of lattice vibrations with an electronic continuum. Note that both electronic background and phonon modes are very similar to the isoelectronic and isostructural compound β-$Na_{0.33}V_2O_5$ at room temperature,[10] indicating that charge dynamics and electron-phonon coupling are of the same nature in both compounds. In order to take into account this coupling, reflectivity and optical conductivity were fitted with the Fano expression,[35]

TABLE I. Fit parameters in cm^{-1} ($\epsilon^{\infty}=6.77$). θ_j is in degrees.

j	$\omega_{TO,j}$	γ_j	$\omega_{p,j}$	θ_j	Remark
1		1524	2825		Drude peak
2	217	46	52	0	
3	333	52	131	20	
4	522	62	210	12	
5	645	94	73	0	
6	3370	2025	7065		Midinfrared band
7	4871	4507	13603		Midinfrared band

$$\sigma(\omega)=\sum_j i\frac{\omega_{p,j}^2}{\gamma_j q_j^2}\frac{(q_j-i)^2}{i+\dfrac{\omega_{TO,j}^2-\omega^2}{\gamma_j\omega}}. \quad (14)$$

The parameter $q_j=-1/\tan(\theta_j/2)$ is the dimensionless Fano parameter of the jth mode, which reflects the degree of asymmetry of the peak (for $\theta_j=0$, a Lorentz line shape is recovered). This approach has been successfully applied to extract phonon properties of FeSi,[36] α'-NaV_2O_5 (Ref. 28), or quantum magnet TiOCl.[37] Fit parameters are summarized in Table I. An overdamped Drude peak and Lorentz oscillators are used to reproduce the flat electronic background and the midinfrared band. Fano profiles are not relevant for the broad peaks at 220 and 647 cm^{-1}. Note that a fit of the modes at 333 and 522 cm^{-1} with usual Lorentz oscillators [Eq. (2)] is of rather poor quality. The two sharp modes at 333 and 522 cm^{-1} have a relatively large Fano parameters resulting from a strong lattice-electronic continuum coupling. Moreover, the positive value of the Fano parameter θ for both modes suggests that phonons interact with electronic states of higher energy.[35]

B. *ac*-plane properties

For the low symmetry *ac* face, the measurement of the reflectivity for at least three polarizations is required to extract the phonon parameters. With the notation of Sec. III, we chose the V2-V2 rung direction as the x axis, as displayed in Fig. 1. Since the V1-V3 and V2-V2 rungs are almost perpendicular, the z axis roughly coincides with the V1-V3 rung direction. The reflectivities $R_{00}(\omega)$, $R_{45}(\omega)$, and $R_{90}(\omega)$ were used to fit the model. As displayed in Fig. 3 a good agreement between the model and the experimental curve is achieved for the three polarizations. The fit parameters are summarized in Table II. The reflectivity $R_{-45}(\omega)$ coincides well with the calculated value deduced from the fit [Fig. 4(a)]. Moreover, Eq. (11) is verified well by experimental data [Fig. 4(b)]. This provides a good support for the model.

Almost all the 22 B_u vibration modes predicted by FGA are found. On the basis of phonon assignment for V_2O_5 (Ref. 38) and α'-NaV_2O_5,[39] B_u modes can be classified as follows:

(1) From 0 to 150 cm^{-1}: chain rotation/translation.
(2) From 150 to 250 cm^{-1}: Sr vibrations.
(3) From 250 to $\approx$500 cm^{-1}: V-O-V bendings.
(4) Above $\approx$500 cm^{-1}: V-O stretchings.

In order to assign the phonon modes, we compared our results to infrared or Raman phonon frequencies and bond lengths in V_2O_5,[38] α'-NaV_2O_5,[39–41] and β-$Sr_{0.33}V_2O_5$,[42] as displayed in Table III. The highest energy modes are usually associated with stretching vibrations of the shortest bonds. The modes at 975/980 cm^{-1} in V_2O_5 and at 939/955 cm^{-1} in α'-NaV_2O_5 are assigned to stretching vibrations of vanadyl bonds of 1.585 and 1.61 Å, respectively. Therefore, we

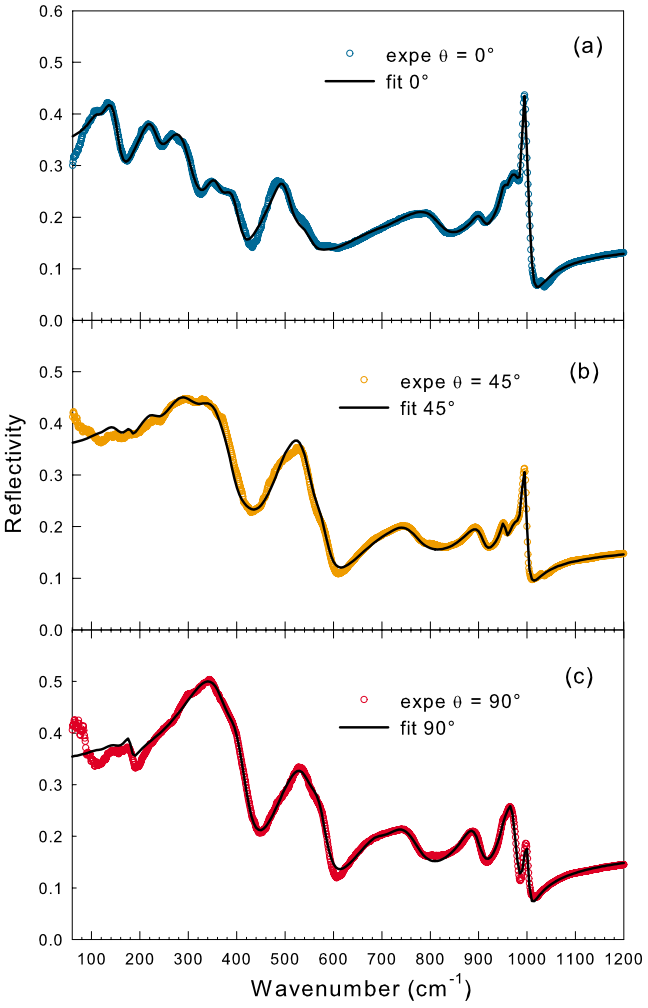

FIG. 3. (Color online) [(a)–(c)] Polarized reflectivities R_{00}, R_{45}, and R_{90} as described in the text. Open circles are experimental curves. Solid lines are the fits.

TABLE II. Fit parameters in cm^{-1} ($\epsilon_{xx}^{\infty}=5.77$, $\epsilon_{xz}^{\infty}=0.23$, and $\epsilon_{zz}^{\infty}=6.62$). θ_i is in degrees. The dipole moment direction close to the vanadyl or V2-O-V2 and V1-O-V3 rung directions are set in bold.

i	$\omega_{TO,i}$	γ_i	θ_i	$\omega_{p,i}$	Remark
1	113	25	−29.00	64	
2	142	38	−24.01	241	
3	179	17	78.08	98	
4	222	48	**−9.17**	264	
5	281	73	**−1.01**	407	
6	332	95	69.89	836	
7	356	45	−39.02	216	
8	390	37	−49.97	268	
9	494	49	−14.56	319	
10	519	61	54.82	517	
11	565	42	**87.75**	221	
12	694	58	−77.01	207	
13	753	96	74.99	460	Unusual damping
14	803	94	−26.99	430	Unusual damping
15	892	48	**−87.27**	345	
16	906	29	**6.40**	184	
17	954	12	21.41	138	
18	963	23	−58.39	420	
19	981	27	**4.40**	287	V1-O4 or V3-O8 stretching
20	992	7	**0.79**	241	V1-O4 or V3-O8 stretching
21	998	9	**−83.66**	159	V2-O6 stretching

assign the modes at 998, 991, and 980 cm^{-1} to V2-O and V1-O4 and/or V3-O8 vanadyl stretchings in β-$Sr_{0.17}V_2O_5$. Indeed, the dipole moment of the 998 cm^{-1} mode is roughly oriented along the V2-O vanadyl direction and is then more likely related to the stretching of this vanadyl. Because V1-O4 and/or V3-O8 vanadyl bonds have almost the same direction, it is not possible to assign separately the 991 and 980 cm^{-1} modes. The modes above 900 cm^{-1} are due to vanadium-oxygen stretching modes, but no more precise conclusion can be drawn on their assignment.

No phonon modes are present in α'-NaV_2O_5 between 940 and 580 cm^{-1}. In V_2O_5, the only mode in this frequency region is attributed to V-O-V stretching. Thus, by comparing the bond lengths with these two compounds (see Table III), the modes between 700 and 800 cm^{-1} in β-$Sr_{0.17}V_2O_5$ can be attributed to in-rung V-O-V stretching vibrations. As shown in Fig. 5, where the diagonal and nondiagonal terms of the optical conductivity are plotted, these modes are quite broad. In particular, the modes at 753 and 803 cm^{-1} have unusually large dampings of $\approx$100 cm^{-1} (Table II). Note that very broad modes are also found around 530–720 cm^{-1} in Raman scattering spectra of β-$Sr_{0.33}V_2O_5$.[42] Since these modes involve an in-rung V-O-V stretching, this suggests a delocalization of 3*d* vanadium electrons over the rung. Indeed, such as in α'-NaV_2O_5, the electrons are expected to be completely delocalized over a rung.[28,30] In this case, their wave function is a linear combination of 3*d* orbitals of both vanadium atoms in the rung and O 2*p* orbitals. This could act as disorder leading to a broadening of phonon modes.[39] Note that such in-rung charge delocalization has been suggested by Popovic *et al.*[42] in β-$Sr_{0.33}V_2O_5$.

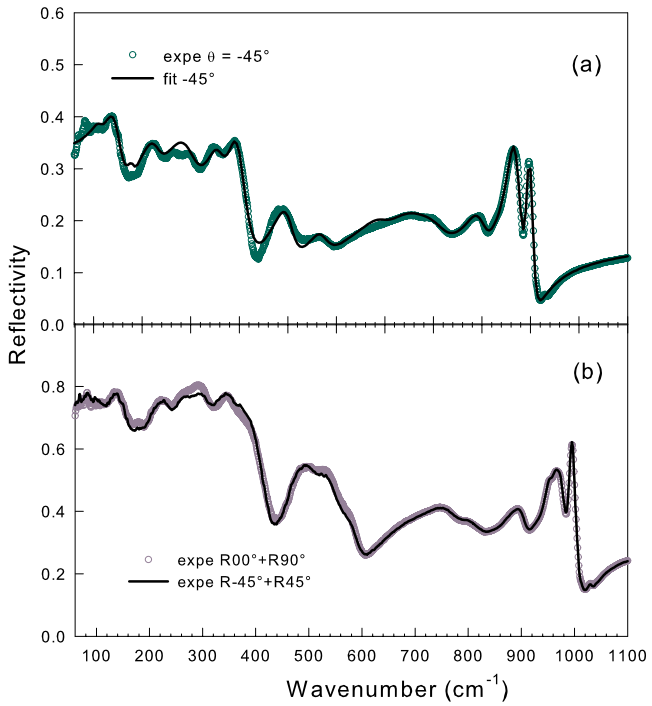

FIG. 4. (Color online) (a) Polarized reflectivity R_{-45}. Open circles are the experimental curve. The solid line is calculated from the fit parameters. (b) Test of the validity of the relation $R_{45}+R_{-45}=R_{00}+R_{90}$.

TABLE III. Comparison between vanadium-oxygen bond lengths and frequencies of stretching modes in $\alpha'-NaV_2O_5$, V_2O_5, and $\beta-Sr_{0.17}V_2O_5$.

V_2O_5[a]				$\alpha'-NaV_2O_5$[b]				$\beta-Sr_{0.17}V_2O_5$		
Bond	Length (Å)	Frequency (cm^{-1})	Remark	Bond	Length (Å)	Frequency (cm^{-1})	Remark	Bond	Length (Å)	Remark
								V2-O5	2.167	
V-O3	2.021	411	V-O3 stretch							
								V3-O7	1.996	
								V1-O5	1.939	In rung
				V-O2	1.912/1.985	469/582				
								V2-O3	1.894	Along *b*
								V3-O7	1.888	Along *b*
V-O3	1.878	506	V-O3 stretch							
							In rung	V1-O2	1.873	Along *b*
				V-O3V	1.82	505	V-O3-V stretch	V1/V3-O5	1.791	In rung
								V2-O1	1.796	In rung
V-O2	1.78	767	V-O2-V stretch							
				V-O1	1.61	939/955	Vanadyl stretch	V3-O8	1.601	Vanadyl
								V2-O6	1.604	Vanadyl
								V1-O4	1.590	Vanadyl
V-O1	1.585	980/975	V-O1 stretch							

[a]Reference 38.
[b]Reference 39.

Another quantity that can be deduced from the model is the Born effective charge tensors. As mentioned above, it is generally not possible to determine the average Born effective charge tensors in ternary compounds. Indeed, $Z_{k,xx}$, $Z_{k,xz}$, and $Z_{k,zz}$ for the oxygen, the strontium, and the vanadium atoms are unknown parameters in Eqs. (10) and (11). However, in $Sr_{0.5}V_6O_{15}$, there is only one Sr for 12 V and 30 O in the unit cell. Moreover, the strontium is much heavier than vanadium or oxygen. Both these arguments allow us to neglect the terms associated with Sr in Eqs. (10) and (11). Within this approximation, we have to solve the following set of equations:

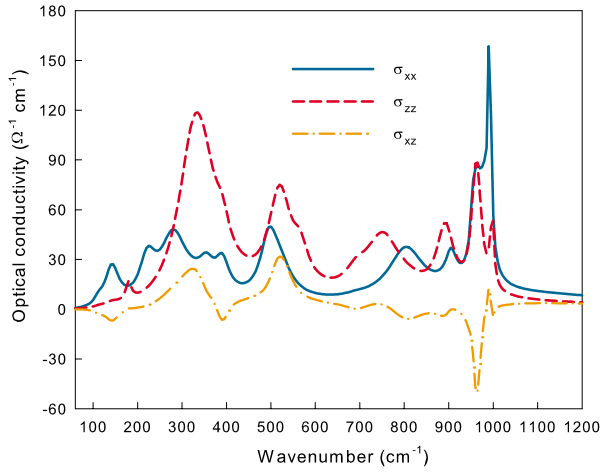

FIG. 5. (Color online) Diagonal and nondiagonal terms of the optical conductivity tensor deduced from the fit.

$$Z_{V,xx}^{*2} + Z_{V,xz}^{*2} = \frac{\mu}{12}\frac{v_c}{4\pi}\sum_i \omega_{p,i}^2 \cos^2\theta_i,$$

$$Z_{V,zz}^{*2} + Z_{V,xz}^{*2} = \frac{\mu}{12}\frac{v_c}{4\pi}\sum_i \omega_{p,i}^2 \sin^2\theta_i,$$

$$Z_{V,xz}(Z_{V,xx} + Z_{V,zz}) = \frac{\mu}{12}\frac{v_c}{4\pi}\sum_i \omega_{p,i}^2 \cos\theta_i \sin\theta_i, \quad (15)$$

where $\mu = \frac{m_V m_O}{\frac{2}{5}m_V + m_O}$. Finally, the average Born effective charge tensors read

$$\hat{Z}_V^* = \begin{pmatrix} 4.47 & 0.14 \\ 0.14 & 5.52 \end{pmatrix}, \quad \hat{Z}_O^* = \begin{pmatrix} -1.79 & -0.06 \\ -0.06 & -2.21 \end{pmatrix}. \quad (16)$$

These tensors can be diagonalized in the system of axis $\{\mathbf{e}_1', \mathbf{e}_2'\}$,

$$\hat{Z}_V^* = \begin{pmatrix} 4.45 & 0 \\ 0 & 5.55 \end{pmatrix}, \quad \hat{Z}_O^* = \begin{pmatrix} -1.78 & 0 \\ 0 & -2.22 \end{pmatrix}, \quad (17)$$

where

$$\mathbf{e}_1' = \begin{pmatrix} 0.99 \\ -0.13 \end{pmatrix} \text{ and } \mathbf{e}_2' = \begin{pmatrix} 0.13 \\ 0.99 \end{pmatrix},$$

which also correspond to a nonrelevant rotation of 1°–2° from the xOz system. The average Born effective charge is clearly anisotropic. The effective charge tensors are almost diagonal in the xOz system. This indicates that the rungs or vanadyl directions are the preferred directions for the dielectric properties.

On the other hand, the high frequency dielectric tensor shows a relatively large anisotropy and is almost diagonal in the xOz system of axes,

$$\hat{\epsilon}_{ac}^{\infty} = \begin{pmatrix} 5.77 & 0.23 \\ 0.23 & 6.62 \end{pmatrix}. \quad (18)$$

Note that the tensor $\hat{\epsilon}_{ac}^{\infty}$ is diagonal in the orthogonal system $\{\mathbf{e}_1, \mathbf{e}_2\}$,

$$\hat{\epsilon}_{ac}^{\infty} = \begin{pmatrix} 5.71 & 0 \\ 0 & 6.67 \end{pmatrix}, \quad (19)$$

where

$$\mathbf{e}_1 = \begin{pmatrix} 0.9694 \\ -0.2455 \end{pmatrix} \text{ and } \mathbf{e}_2 = \begin{pmatrix} 0.2455 \\ 0.9694 \end{pmatrix},$$

which correspond to a small rotation of −4° to −5° from the xOz system. Thus, ac-plane high frequency dielectric properties should be related to the V2-O-V2 and V1-O-V3 rung directions.

V. CONCLUSION

Phonon dynamics was explored from reflectivity spectra along the b axis and on the ac face of a monoclinic β-$Sr_{0.17}V_2O_5$. Of the 11 A_u modes predicted by the factor group analysis along the b axis, only two large modes and two very broad peaks are observed. Moreover, phonon modes show asymmetric line shapes. This suggests that lattice vibrations interact with an electronic continuum. A good fit of the optical conductivity is achieved by using Fano profiles. The obtained values for the asymmetry Fano parameters indicate that the typical energy scale of the electronic states coupled to phonon is larger than the phonon energy. Because of the low symmetry, the dielectric function cannot be obtained from a usual Drude-Lorentz fit of the reflectivity. Actually, tensor dispersion formulas must be used and reflectivity must be measured for three polarization directions. This model provides a very good fit of experimental results and allows us to extract accurately phonon parameters, including dipole moment directions. Phonon modes assigned to in-rung V-O-V stretching vibrations are found to be unusually damped. This is interpreted as a signature of charge delocalization within molecular orbitals on the rungs. Moreover, both high frequency dielectric tensor and Born effective charge tensors, obtained from the model, can be diagonalized by choosing a system of axis parallel (perpendicular) to the V-O-V rung directions. Thus, dielectric properties are more related to V-O-V rung directions than to the crystallographic axis, as suggested by extended Hückel tight binding calculations.

ACKNOWLEDGMENTS

The authors thank A. B. Kuz'menko for helpful discussions on the model for dielectric tensor calculation and for providing us his program REFFIT, and F. Gervais for a critical reading of the manuscript.

[1] *Strong Interactions in Low Dimensions*, in Physics and Chemistry of Materials With Low-Dimensional Structures Vol. 25, edited by D. Baeriswyl and L. Degiorgi (Kluwer Academic, Dordrecht, 2004).
[2] H. Fehske, G. Wellein, G. Hager, A. Weisse, and A. R. Bishop, Phys. Rev. B **69**, 165115 (2004).
[3] S. Biermann, A. Georges, A. Lichtenstein, and T. Giamarchi, Phys. Rev. Lett. **87**, 276405 (2001).
[4] M. Imada, A. Fujimori, and Y. Tokura, Rev. Mod. Phys. **70**, 1039 (1998).
[5] H. Yamada and Y. Ueda, J. Phys. Soc. Jpn. **68**, 2735 (1999).
[6] Y. Ueda, J. Phys. Soc. Jpn. **69**, 149 (2000).
[7] T. Yamauchi, Y. Ueda, and N. Mori, Phys. Rev. Lett. **89**, 057002 (2002).
[8] Y. Ueda, M. Isobe, and T. Yamauchi, J. Phys. Chem. Solids **63**, 951 (2002).
[9] M. Itoh, N. Akimoto, H. Yamada, M. Isobe, and Y. Ueda, J. Phys. Chem. Solids **62**, 351 (2001).
[10] C. Presura, M. Popinciuc, P. H. M. van Loosdrecht, D. van der Marel, M. Mostovoy, T. Yamauchi, and Y. Ueda, Phys. Rev. Lett. **90**, 026402 (2003).
[11] Z. V. Popovic, M. J. Konstantinovic, V. V. Moshchalkov, M. Isobe, and Y. Ueda, J. Phys.: Condens. Matter **15**, L139 (2003).
[12] C. Sellier, F. Boucher, and E. Janod, Solid State Sci. **5**, 591 (2003).
[13] T. Yamauchi, H. Ueda, J. I. Yamaura, and Y. Ueda, Phys. Rev. B **75**, 014437 (2007).
[14] P. H. M. van Loosdrecht, C. Presura, M. Popinciuc, M. Mostovoy, G. Maris, T. T. M. Palstra, P. J. M. van Bentum, H. Yamada, T. Yamauchi, and Y. Ueda, J. Supercond. **15**, 587 (2002).
[15] C. A. Kuntscher, S. Frank, I. Loa, K. Syassen, T. Yamauchi, and Y. Ueda, Phys. Rev. B **71**, 220502(R) (2005).

[16] K. Okazaki, A. Fujimori, T. Yamauchi, and Y. Ueda, Phys. Rev. B **69**, 140506(R) (2004).
[17] S. Sirbu, T. Yamauchi, Y. Ueda, and P. H. M. van Loosdrecht, Eur. Phys. J. B **53**, 289 (2006).
[18] Y. Ueda, H. Yamada, M. Isobe, and T. Yamauchi, J. Alloys Compd. **317-318**, 109 (2001).
[19] M. Itoh, I. Yamauchi, T. Kozuka, T. Suzuki, T. Yamauchi, J.-I. Yamaura, and Y. Ueda, Phys. Rev. B **74**, 054434 (2006).
[20] I. Yamauchi, M. Itoh, T. Yamauchi, and Y. Ueda, Phys. Rev. B **74**, 104410 (2006).
[21] J.-I. Yamaura, M. Isobe, H. Yamada, T. Yamauchi, and Y. Ueda, J. Phys. Chem. Solids **63**, 957 (2002).
[22] M. L. Doublet and M. B. Lepetit, Phys. Rev. B **71**, 075119 (2005).
[23] J. B. Goodenough, J. Solid State Chem. **1**, 349 (1970).
[24] T. Erata, T. Takahashi, and H. Nagasawa, Solid State Commun. **39**, 321 (1981).
[25] H. Nagasawa, T. Takahashi, T. Erata, M. Onoda, Y. Kanai, and S. Kagoshima, Mol. Cryst. Liq. Cryst. **86**, 195 (1982).
[26] M. Heinrich, H.-A. Krug von Nidda, R. M. Eremina, A. Loidl, Ch. Helbig, G. Obermeier, and S. Horn, Phys. Rev. Lett. **93**, 116402 (2004).
[27] V. T. Phuoc, C. Sellier, and E. Janod, Phys. Rev. B **72**, 035120 (2005).
[28] A. Damascelli, D. van der Marel, M. Gruninger, C. Presura, T. T. M. Palstra, J. Jegoudez, and A. Revcolevschi, Phys. Rev. Lett. **81**, 918 (1998).
[29] A. Damascelli, C. Presura, D. van der Marel, J. Jegoudez, and A. Revcolevschi, Phys. Rev. B **61**, 2535 (2000).
[30] N. Suaud and M. B. Lepetit, Phys. Rev. Lett. **88**, 056405 (2002).
[31] C. Sellier, Ph.D. thesis, University of Nantes, 2004.
[32] M. Born and K. Huang, *Dynamical Theory of Crystal Lattices* (Clarendon, Oxford, 1956).
[33] A. B. Kuz'menko, D. van der Marel, P. J. M. van Bentum, E. A. Tishchenko, C. Presura, and A. A. Bush, Phys. Rev. B **63**, 094303 (2001).
[34] A. B. Kuz'menko, E. A. Tishchenko, and V. G. Orlov, J. Phys.: Condens. Matter **8**, 6199 (1996).
[35] U. Fano, Phys. Rev. **124**, 1866 (1961).
[36] A. Damascelli, K. Schulte, D. van der Marel, and A. A. Menovsky, Phys. Rev. B **55**, R4863 (1997).
[37] G. Caimi, L. Degiorgi, N. N. Kovaleva, P. Lemmens, and F. C. Chou, Phys. Rev. B **69**, 125108 (2004).
[38] P. Clauws, J. Broeckx, and J. Vennik, Phys. Status Solidi B **131**, 459 (1985).
[39] Z. V. Popovic, M. J. Konstantinovic, R. Gajic, V. Popov, Y. S. Raptis, A. N. Vasil'ev, M. Isobe, and Y. Ueda, J. Phys.: Condens. Matter **10**, L513 (1998).
[40] Z. V. Popovic, M. J. Konstantinovic, R. Gajic, V. Popov, Y. S. Raptis, A. N. Vasil'ev, M. Isobe, and Y. Ueda, Solid State Commun. **110**, 381 (1999).
[41] Z. V. Popovic, M. J. Konstantinovic, R. Gajic, V. N. Popov, M. Isobe, Y. Ueda, and V. V. Moshchalkov, Phys. Rev. B **65**, 184303 (2002).
[42] Z. V. Popovic, A. G. Kontos, Y. S. Raptis, M. Isobe, and Y. Ueda, J. Phys.: Condens. Matter **18**, 7779 (2006).